Development of a cryogenic FTIR system for measuring very small attenuation coefficients of infrared materials

Sayumi Kaji[a], Yuki Sarugaku[b,c], Yuji Ikeda[c,d], Kenshi Nakanishi[c], Naoto Kobayashi[c,e], Sohei Kondo[c], Takayuki Arasaki[c], and Hideyo Kawakita[a,c]

[a]Department of Physics, Faculty of Science, Kyoto Sangyo University, Motoyama, Kamigamo, Kita-ku, Kyoto 603-8555, Japan;
[b]Kiso Observatory, Institute of Astronomy, University of Tokyo, 10762-30 Mitaka, Kiso-machi, Kiso-gun, Nagano 397-0101, Japan;
[c]Laboratory of Infrared High-resolution spectroscopy (LiH), Koyama Astronomical Observatory, Kyoto Sangyo University, Motoyama, Kamigamo, Kita-ku, Kyoto 603-855, Japan;
[d]Photocoding, 460-102 Iwakura-Nakamachi, Sakyo-ku, Kyoto 606-0025, Japan;
[e]Institute of Astronomy, University of Tokyo, 2-21-1 Osawa, Mitaka, Tokyo 181-0015,Japan

ABSTRACT

We have been working on a longterm project for developing a variety of infrared immersion gratings for near- to mid-infrared wavelengths. The transmittance of material is essential to realize high-efficiency immersion gratings for astronomical applications. For a typical grating, the attenuation coefficient α_{att} must be <0.01 cm^{-1} for the absolute diffraction efficiency of >70%. However, as there are few reports of $\alpha_{att} < 0.01$ cm^{-1} for infrared optical materials in the literatures, we performed high-accuracy measurements of α_{att} for a variety of infrared materials applicable to immersion gratings. We have already reported α_{att} at room temperature for single-crystal Si, single-crystal Ge, CVD-ZnS, CVD-ZnSe, and high-resistivity single-crystal CdZnTe (Ikeda et al. 2009[7], Kaji et al. 2014[10], and Sarugaku et al. 2016[9]). Next, we proceeded with the measurements of α_{att} at cryogenic temperatures of 20–80 K range, which is the typical operational temperatures of infrared instruments, and for which the shifts of the band gap and/or the sharpness of the lattice absorption lines from the corresponding room temperature values are expected. Thus, we developed a new cryogenic FTIR system that enables high-accuracy measurements at cryogenic temperatures. The system has a mechanism with which two sample cells and a reference cell can be easily and quickly switched without any vacuum leak or temperature change. Our preliminary measurement of Ge using this cryogenic FTIR system found that both the cut-on and cut-off wavelengths shift to the shorter (from 2.0 to 1.7 μm) and longer (from 10.6 to 10.9 μm) wavelengths, respectively, when the temperature is decreased from room temperature to the cryogenic temperature (<28 K). We plan to complete cryogenic measurements for a variety of infrared materials by the end of 2016.

Keywords: immersion grating, infrared material, attenuation coefficient, absorption coefficient, infrared, high-resolution, cryostat, transmittance, absorption

1. INTRODUCTION

Immersion grating is a type of diffraction grating with the immersed diffraction surface in an optical material having a high refractive index of $n > 2$[2]. As the wavelength in the material is reduced to $1/n$, an immersion grating can provide a spectral resolution n times higher than that of a classical reflective grating with the same clear aperture, or can reduce the diameter of the collimated beam Φ, namely the instrumental volume, by a factor of n compared to a classical reflective grating with the same spectral resolution. Thus, immersion gratings are useful for building high-resolution spectrographs with $R \geq 50{,}000$ for ground-based 30-m class telescopes and realizing airborne spacecraft spectrographs with $R \geq 20{,}000$ in the infrared wavelength region.

Our group belongs to Laboratory of Infrared High-resolution spectroscopy (LiH) at Koyama Astronomical Observatory of Kyoto Sangyo University*, Japan, and has been working on a longterm project for the development of a variety of infrared immersion gratings for near- to mid-infrared wavelengths. In this project, we have comprehensively studied the

*LiH: http://merlot.kyoto-su.ac.jp/LIH/index.html processing techniques for obtaining ultrafine groove shape[1-6], the selection of suitable materials for immersion gratings[7-10], the development of coating techniques[3-5,8,9,11], and the design and assembly of spectrographs using immersion gratings[1,12-20]. This paper focuses on material selection.

For a high-efficiency immersion grating, the transmittance of material is essential for application of the grating in astronomy because when the typical optical path length in the immersion grating becomes >100 mm, a significant degradation of the total efficiency occurs even for a very small attenuation (a total energy loss of ~10% is expected for a Ge immersion grating with an assumed attenuation coefficient of $\alpha_{att} = 0.01$ cm^{-1} for a spectral resolution $R = 100{,}000$ at $\lambda = 8$ µm). However, there have been few reports of infrared materials with $\alpha_{att} < 0.01$ cm^{-1}. Therefore, we performed high-accuracy measurements of the attenuation coefficients α_{att} for a variety of infrared optical materials with $n > 2$ that are applicable to immersion gratings. We have previously reported some results on α_{att} at room temperature. Ikeda et al. (2009) revealed that both CVD-ZnS and CVD-ZnSe materials showed $\alpha_{att} = 0.01$–0.03 cm^{-1} at 0.9–0.6 µm, and single-crystal Si shows $\alpha_{att} \leq 0.001$ cm^{-1} at 1.3–1.6 µm[7]. Kaji et al. (2014) suggested usable wavelength ranges for several materials as immersion gratings based on the measurements between 1.3 and 20 µm using a custom-improved high-accuracy FTIR system[10]; near-infrared wavelengths (2–5 µm) were suggested for single-crystal Si and CVD-ZnS, thermal infrared wavelengths (3–10 µm) were suggested for single-crystal Ge and CVD-ZnSe, and mid-infrared wavelengths (5–20 µm) were suggested for high-resistivity single-crystal CdZnTe. Sarugaku et al. (2016) proposed that the attenuation of high-resistivity single-crystal CdZnTe could originate from Mie scattering by the sub-µm size of Te particles[9].

Next, we proceeded with the measurements of α_{att} at cryogenic temperatures of 20–80 K that are the typical operational temperatures. For these measurements, the shifts of the band gap and/or the sharpness of the lattice absorption lines from the corresponding room temperature values are expected (e.g., Hawkins 1998[21]). Even a small difference can critically influence the design of an instrument (for the optimum wavelength region) and the science cases, because the measurable atomic and molecular lines change. Therefore, in this paper, we describe the details of the cryogenic FTIR system developed by us and the testing results in section 2 and 3, respectively, and report the preliminary result obtained for the attenuation coefficients of single-crystal Ge at cryogenic temperatures in section 4.

2. CRYOGENIC FTIR SYSTEM

2.1 Requirements

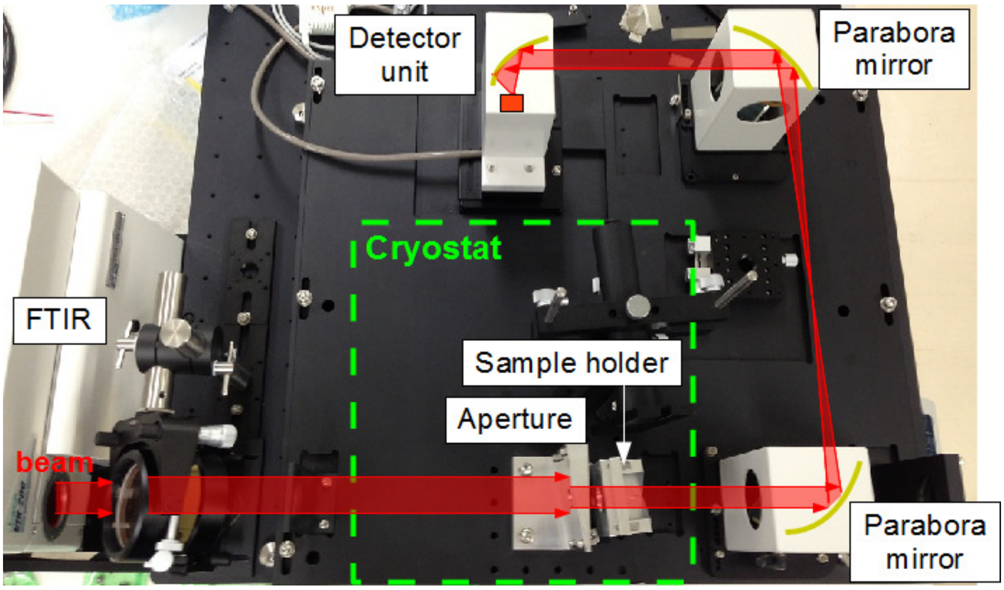

Figure 1. High-accuratcy FTIR system for measurements of internal attenuations of infrared materials at room temperature (Kaji et al. 2014[10]). The newly developed cryostat unit is located within a box drawn by the dashed line.

To enable the measurements of the attenuation coefficients for infrared optical materials at cryogenic temperatures, we attached a new cryostat unit for cooling the samples to the current high-accuracy FTIR system that was originally developed for performing measurements at room temperature, as reported by Kaji et al. (2014)[10]. The newly built unit was inserted in a space between the aperture and the first off-axis parabola mirror, where the collimated beam is propagated (see Figure 1). Table 1 shows the requirements that must be satisfied by the new cryostat. For the high-accuracy measurement, we employ "a double sample method" that was used for measurements at room temperature by Ikeda et al. (2009) [7] and Kaji et al. (2014) [10]. Because this method requires the measurements of two samples (a thick sample and a thin sample) in addition to that of the reference (no sample), three samples cells that can be quickly switched during a single heat cycle must be provided.

Table 1. Requirements of the new cryostat for sample cooling

Item	Specifications
Beam height	90 mm
Size of the windows	>Φ 12 mm (for clear aperture)
Wavelength	1.3–20 μm
Physical size	<340 mm (W) × 245 mm (L) × 340 mm (H)
Total weight	<30 kg
Minimum temperature of measurement	20 K
Maximum time for cooling	<2 days
Number of sample cells	3
Positional repeatability of samples	<0.5 mm
Measurement method	Double sample method (Ikeda et al. (2009) [7] and Kaji et al. (2014) [10]

2.2 Thermal design

The most challenging requirement for this cryostat system is that the samples must be cooled to temperatures below ~20 K with a stability of ± 0.1 K despite the presence of two large windows required for the entrance and exit beams. Assuming that the ambient environment is a black body at 300 K, the thermal radiative inflows from those windows to the inside are calculated to be relatively large (0.42 W). Thus, a careful and quantitative thermal design is crucial.

To achieve a quantitative thermal design, we used a thermal-flow block diagram of our cryostat (Figure 2). This diagram simulates thermal flows between the parts in the cryostat. In the diagram, we present an expected mechanical part with no temperature gradient as one block. The thermal flows between the parts are shown with connecting arrows. We consider the thermal conduction (shown with dashed lines) and the thermal radiation (shown with solid lines) as the thermal flows. While the surface area and the emissivity are defined for each block, the thermal conductivity is defined for each connecting arrow. Assuming that the temperatures of the ambient environment and the cryocooler cold head or the thermal inflows and outflows are the boundary conditions of system, the equilibrium temperature and the thermal inflows/outflows between the parts can be calculated. Therefore, using this diagram, we can optimize the surface areas and emissivities (i.e., the material) of the parts and the conductivities (i.e., the material, length, and cross section) of the connecting arrows to achieve the target temperature of the sample holder at 20 K.

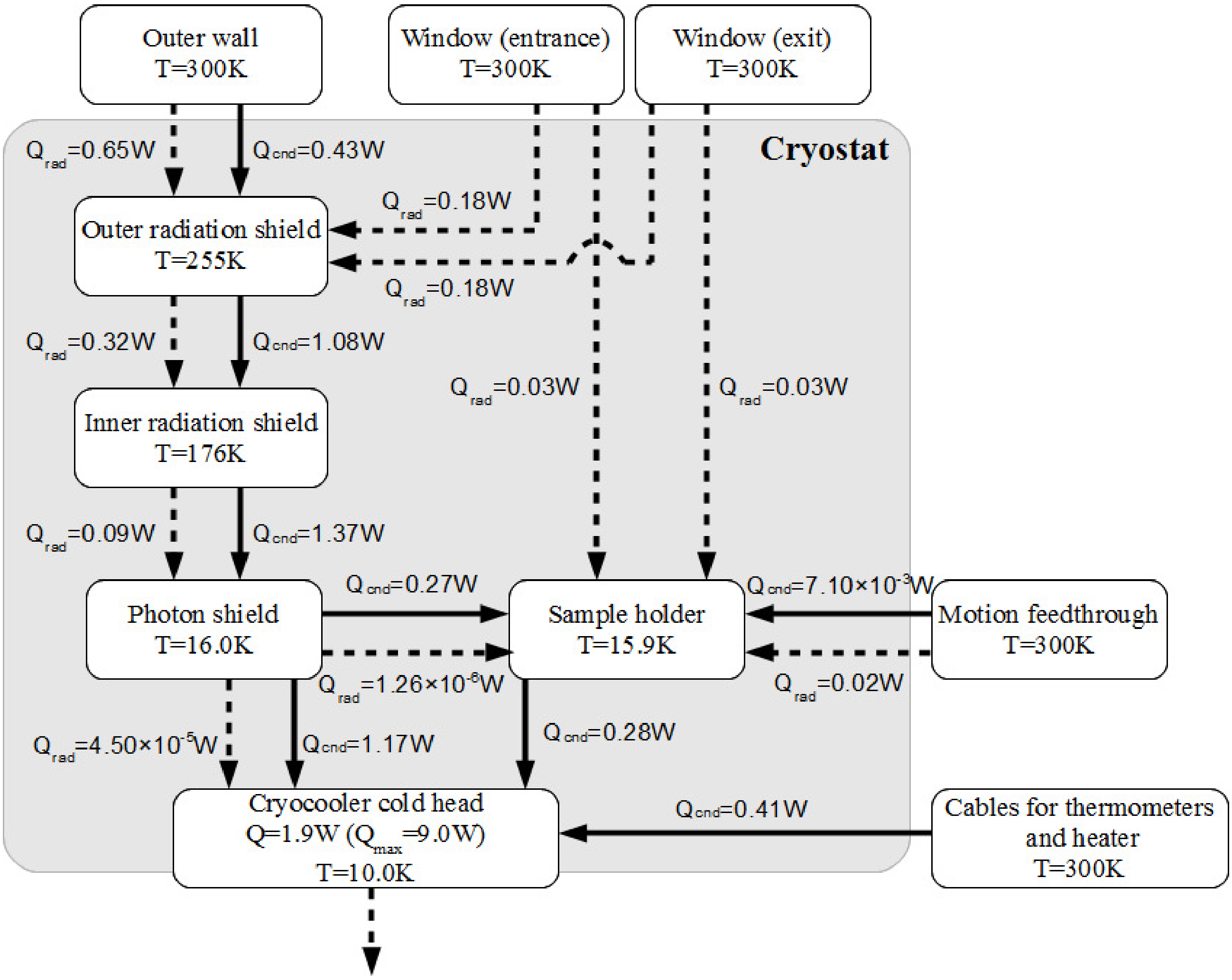

Figure 2. Thermal-flow block diagram for thermal design. Each box represents a mechanical part expected to have a single temperature in the cryostat. Lines connecting boxes show thermal flows: solid lines represent radiation, and dashed lines represent thermal conduction. Assumed emissivity and conductivity values for each part are given in Table 2.

To perform the actual optimization, we adopted 300 K as the ambient temperature, 10 K as the cold head temperature of the cryocooler, and 9.0 W as the cooling power of cryocooler, with the temperature and power of the cryocooler taken from the values in the catalogue by Sumitomo Heavy Industries, Ltd. Table 2 shows the final thermal design. Even with the very small thermal inflow to the cryocooler of 1.9 W (which is less than 1/4 of the maximum power), we obtained a solution for cooling the sample holders to 16 K. As expected, it was critical to suppress the radiative inflows of the ambient thermal radiation. The temperature at the sample holder is achieved by using “three radiation shields (outer and inner radiation shields, and photon shield).” Each radiation shield is supported with three glass epoxy legs with a low thermal conductivity of 0.5 W m^{-1} K^{-1} in order to prevent the temperatures of the radiation shields from effectively increasing.

Table 2. Assumed and obtained parameters of each block after optimization.

	Material	Emissivity	Thermal conductivity [W m^{-1} K^{-1}]	Effective surface area [m^2]	Cross section [m^2]× length [m]	Remarks
Outer wall	A6061-T6	0.1	-	0.41	-	-
Outer Radiation shield	SUS304	0.07	-	0.29	-	-
Inner Radiation shield	SUS304	0.07	-	0.26	-	-
Photon shield	SUS304	0.07	-	0.09	-	-
Cold work surface	Oxygen-free copper C1020	0.05	-	0.01	-	-
Cold plate	Oxygen-free copper C1020	0.05	-	6.0×10^{-3}	-	-
Entrance window	KBr	1	-	6.2×10^{-4}	-	-
Exit window	KBr	1		6.2×10^{-4}	-	-
Cryocooler cold head	OFHC-copper	-	-	3.4×10^{-3}	-	-
Cables	Copper	-	401@273K	-	$1.3\times10^{-7}\times 0.25$	Including 7 cables
Support poles	Glass epoxy	-	0.5	-	$6.4\times10^{-5}\times 0.011$	Including 9 poles

2.3 Mechanical design

Figure 3 shows the mechanical design of the new cryogenic unit. The dimensions of the cryostat are 327 mm (W) × 240 mm (L) × 270 mm (H), and its weight including the inside sample switcher unit and the cryocooler cold head is approximately 28 kg. These physical parameters satisfy the requirements described in section 2.1. The thermal radiation from the ambient environment is reduced by inner and outer radiation shields as well as by the photon shield. The sample switcher unit is located in the space that is entirely surrounded by the photon shield. This unit comprises an oil-free linear motion guide (SR15MSW produced by THK Co., Ltd.), a rotary/linear motion feedthrough (FCH025-H produced by INFICON Co., Ltd.), a roller plunger (CBPJ9 bought from MISUMI Inc.), and the custom-made sample holders, cold work surface, and guide-wall (see Figure 4). As the sample holders are located on the linear motion guide together with the cold work surface, we can easily and quickly switch the samples from the outside of the cryostat by hooking the tip of the motion feed through to the linear motion guide, and pulling or pushing it (see Figure 4 and 5). Because the linear motion feedthrough can be thermally detached from the cold work surface, there is no direct thermal inflow from the outside. To realize good positional repeatability for the sample holders (<0.5 mm) in the switching, we use the roller plunger with a bearing on the side of the cold work surface (in Figure 5). This roller plunger is designed to continue to push the guide wall with the tensile force applied by the spring contained in the plunger. The guide-wall has three grooves that correspond to the positions of the two samples and the reference, wherein the roller plunger falls in the grooves with the restoring force and can be accurately fixed at the aiming position with a good positional repeatability.

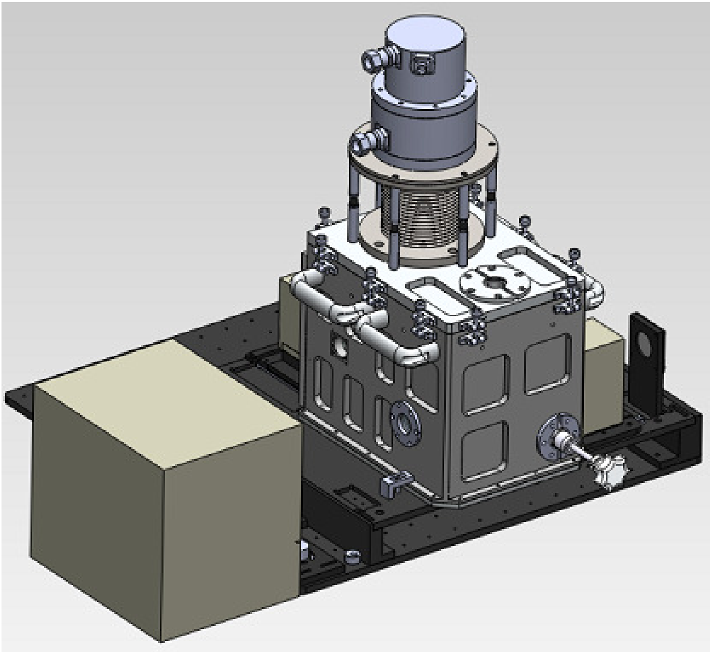

Figure 3. 3D drawing of the newly developed cryogenic unit attached to the FTIR system.

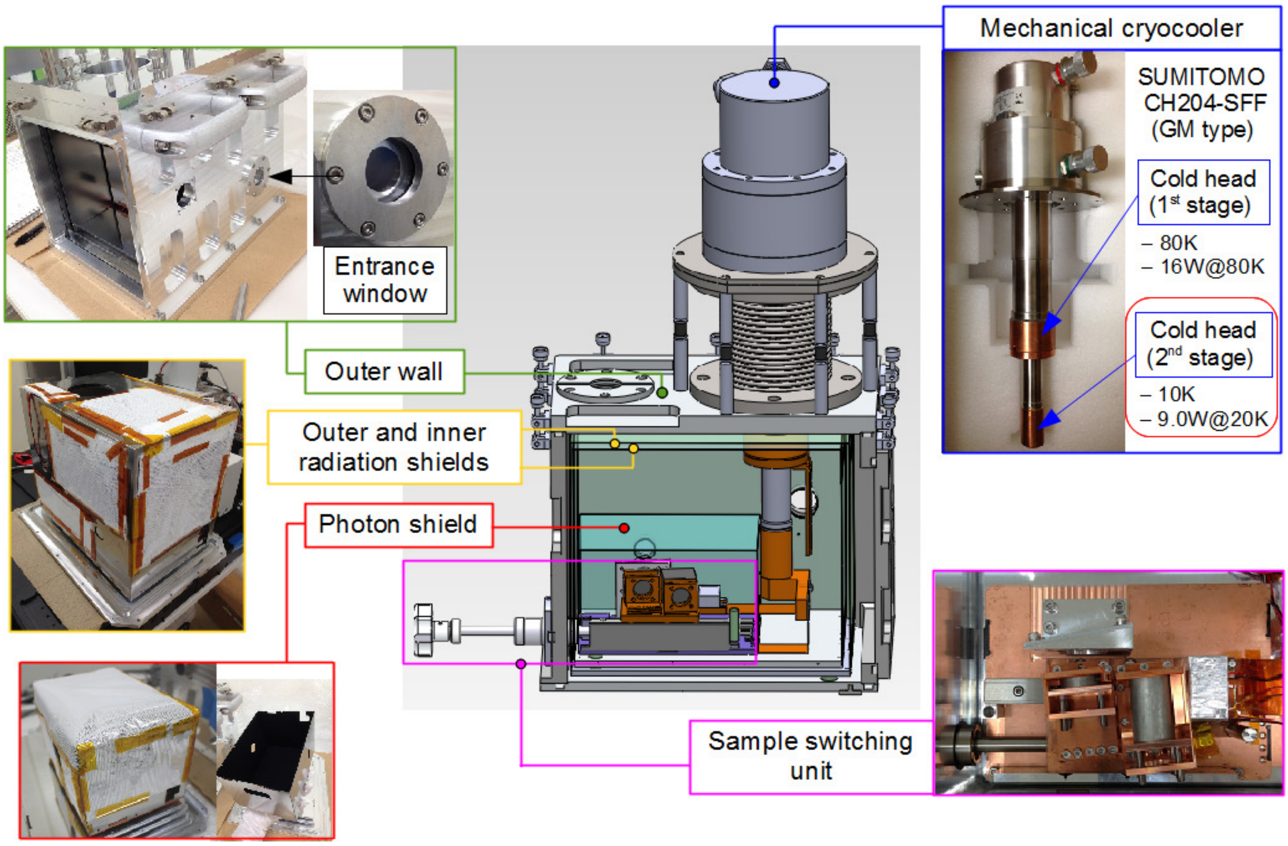

Figure 4. Inner structure of the cryostat.

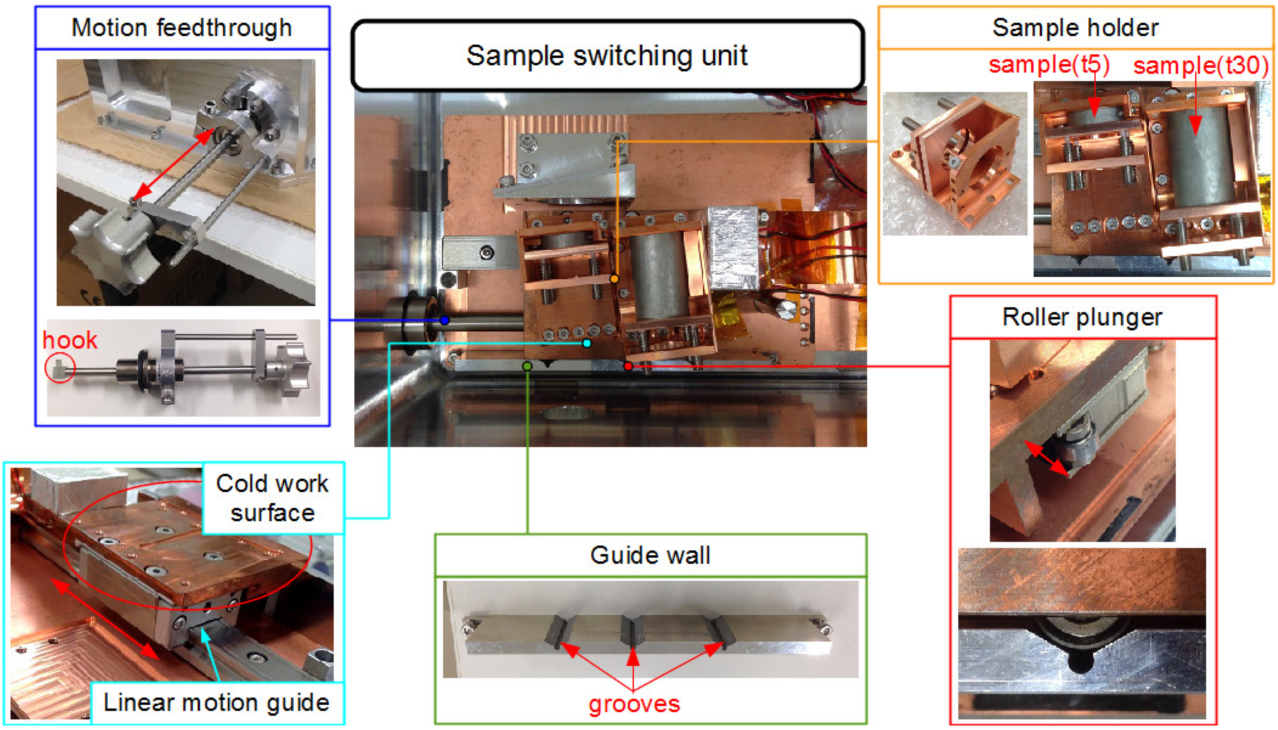

Figure 5. The mechanical structures of the sample switching unit.

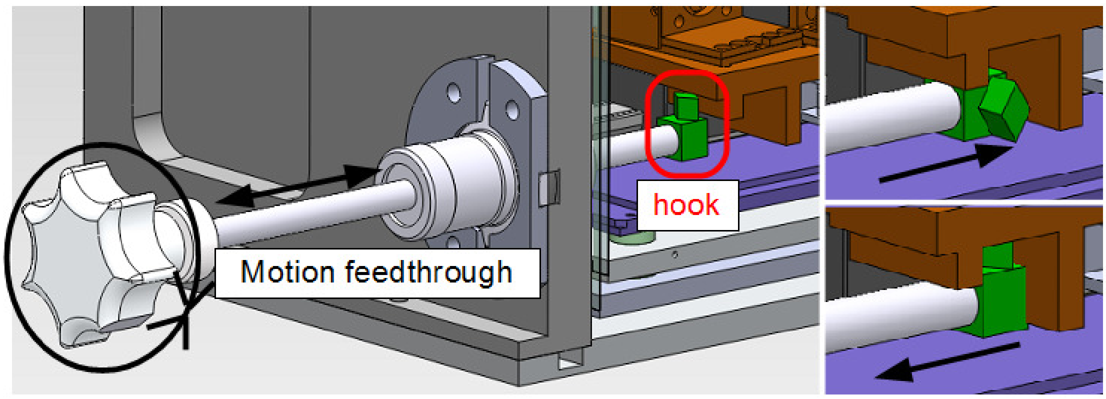

Figure 6. Mechanism of feedthrough and hook for sample switching. First, the hook (colored in green) at the tip is inserted into the claw under the cold work surface on the linear motion guide (colored in orange) by rotating the motion feedthrough (colored in silver). Then, the sample holders together with the cold work surface are moved by pushing or pulling of the motion feedthrough.

2.4 Optical design

We selected KBr as the material for entrance and exit windows because KBr transmits wavelengths of 1.3–20 μm with a transparency of ~80%. Although the most of energy loss is generated by Fresnel reflection on the surface, we use the window without anti-reflection coating in order to suppress the condensation of the atmospheric water on the window. The dimensions of the windows are Φ 45 mm × t 8 mm with a clear aperture of Φ 28 mm.

The maximum flexure by the atmospheric pressure and the maximum bending of the optical bench by the self-weight of the cryostat are calculated to be 0.1 μm and 0.31 mm, respectively. Although these produce an optical aberration of the focused beam on the FTIR detector and the miss-alignment of the optical train, we confirmed by using the ray tracing that both these effects are negligible.

3. FABRICATION AND TESTING

Figure 7 shows time variations of the pressure and the temperature in the cryostat during a testing run. Temperatures at the cryocooler cold head, the cold work surface, the photon shield, and the outer and inner radiation shields were measured using the Si diode temperature sensors (DT-670 produced by Lake Shore Cryotronics, Inc.), and the power-on/off timings of the cryocooler are indicated with triangles. The ambient temperature, controlled by the air-conditioner, was approximately 20°C. It took approximately one day for the sample holder to reach the equilibrium temperature, satisfying the requirement for the cooling time to be less than two days (see Table 1). The lowest attained temperatures of various parts in the cryostat are shown in Table 3. The temperature of the cold work surface did not reach the required temperature of 20 K, probably because the cryocooler cold head could not reach the operating temperature (=10 K) guaranteed by the developer. In addition, the detected FTIR signals were found to be slightly unstable because of the influence of vibrations propagated from the cryocooler to the FTIR unit. After detailed investigations, we plan to fix these problems to enable more accurate measurements.

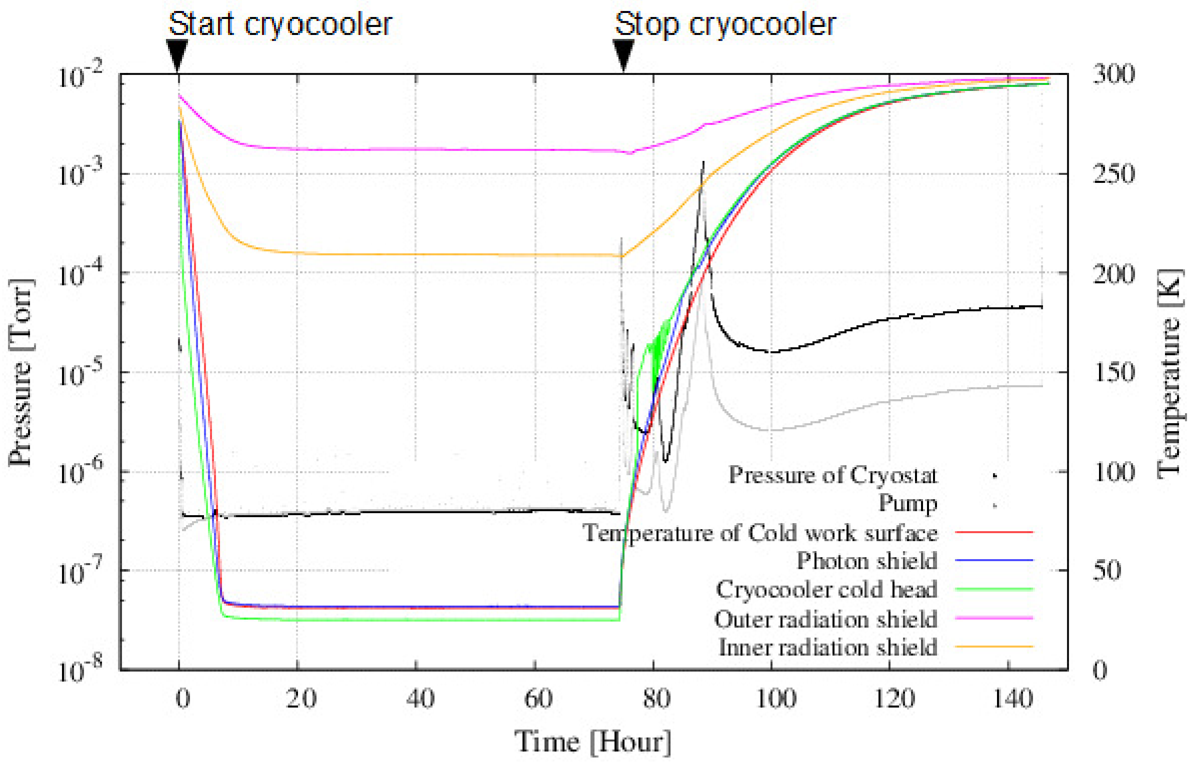

Figure 7. Time variations of the pressure and temperature in the cryostat during a testing run from March 4th, 2016.

Table 3. End-point temperature of each component

	Target [K]	Designed [K]	Measured [K]
Cryocooler cold head	10	10	25
Cold work surface	20	17	29
Photon shield	20	17	32
Inner radiation shield	200	175	206
Outer radiation shield	260	255	259

4. PRELIMINARY RESULT

We measured the attenuation coefficient of the single-crystal Ge produced by TDY Inc. that has already been measured at room temperature. The dimensions of the two samples were Φ 20 mm × t 30 mm and Φ 20 mm × t 5 mm. The attenuation coefficient is derived from equation (2) in the work of Kaji et al. (2014) [10] using the transmittances of thin (t 5 mm) and thick (t 30 mm) samples. The wavelength range was from 1.3 to 28 μm (7800–350 cm^{-1}), and the spectral resolution was 4 cm^{-1}. To improve the signal to noise (S/N) ratio, we obtained 1,280 spectra for one sample. During the measurements, we turned off the power of the cryocooler in order to minimize the influence of the vibration propagated from the cryocooler to the FTIR instrument (see the previous section). The temperature variation due to the temporal turning-off of the cryocooler is estimated to be <15 K.

Figure 8 shows the preliminary result for the attenuation coefficients of Ge at the cryogenic temperature (blue circles). We also plotted our previous results obtained at room temperature as well as the absorption coefficient values given in the literature. Even though we encountered a problem during the measurements in that the thermometer came off the sample holder, the temperature was estimated to be at most 28 K based on the temperatures measured by this thermometer during other cooling runs. In Figure 8, the cut-on wavelength, defined as the shortest wavelength for α_{att} < 0.01 cm^{-1}, shifts from 2.0 μm (at room temperature) to 1.7 μm (at cryogenic temperature). This indicates that at cryogenic temperatures, Ge immersion grating can cover the entire K-band (2.0–2.4 μm), including the longer wavelength region of the H-band (1.5–1.8 μm). In addition, the cut-off wavelength, defined as the longest wavelength for α_{att} < 0.01 cm^{-1}, shifts from 10.6 μm (at room temperature) to 10.9 μm (at cryogenic temperature) with the decrease of the attenuation coefficients by a factor of ~3 and the sharpness of the lattice absorption lines. The wavelength dependence of the attenuation coefficient around the cut-off wavelength is in good agreement with the results at 20 K reported by Fray et al. (1965) [23]. It is found that Ge immersion grating cannot cover the entire N-band (8–13 μm) even at the cryogenic temperatures.

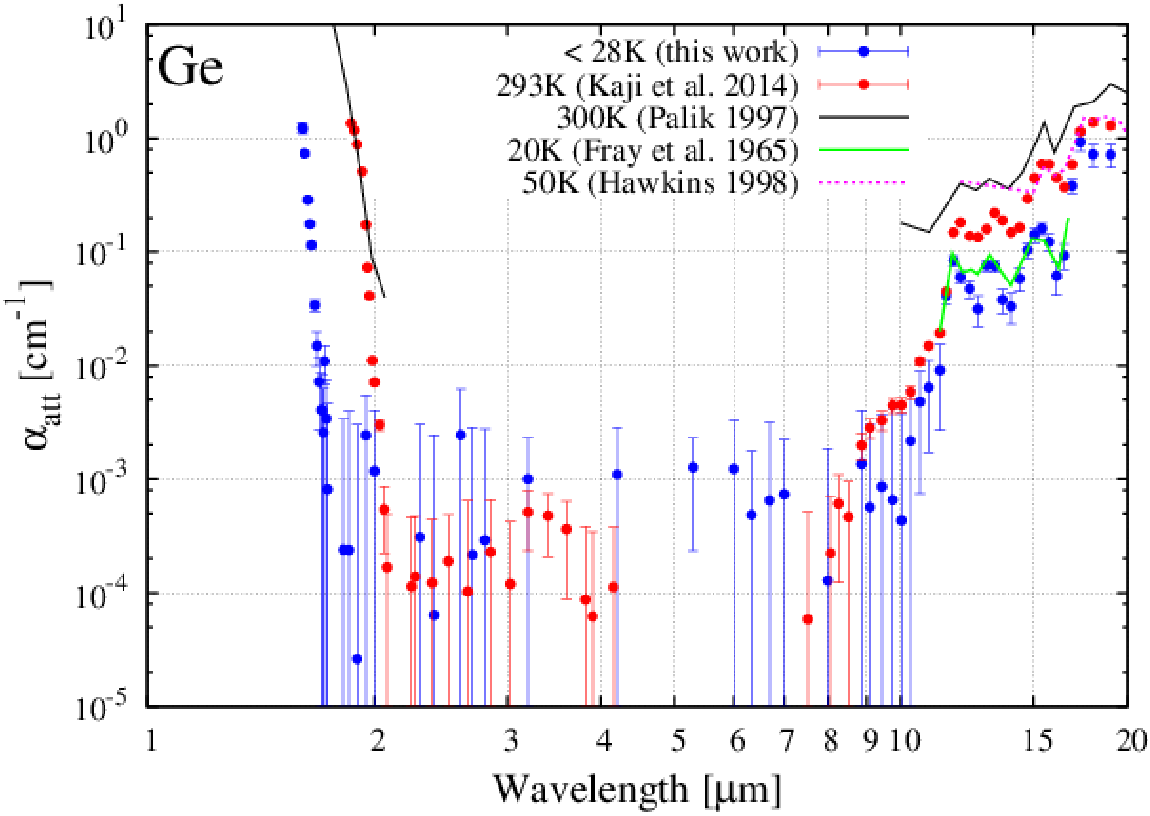

Figure 8. Attenuation coefficients at cryogenic temperature (blue circles). Red circles show the results at room temperature obtained by Kaji et al. (2014) [10]. Black lines and green lines show the measurements in the literatures at 300 K (Palik 1997[22]) and 20 K (Fray et al. 1965 [23]). Magenta dashed lines show absorption coefficients theoretically predicted by Hawkins (1998) [21].

5. SUMMARY

We are working on a project to measure the attenuation coefficients of a variety of infrared optical materials at cryogenic temperatures in order to select materials that are suitable for use in immersion gratings. For this purpose, we developed a new cryogenic unit that can be attached to the current FTIR system used for measurement at room temperature. Using an originally designed sample switching unit that enables us to switch two samples cells and a reference cell easily and quickly without any vacuum leak or temperature change, we achieved high-accuracy measurements of the attenuation coefficients at cryogenic temperatures using “the double sample method.” In our preliminary result for Ge that were obtained using this system, both the cut-on wavelength and the cut-off wavelength are shifted from 2.0 μm (at room temperature) to 1.7 μm (at cryogenic temperature), and from 10.6 μm (at room temperature) to 10.9 μm (at cryogenic temperature) with the decrease of the attenuation coefficients by a factor of ~3 and the sharpness of the lattice absorption lines, respectively. The wavelength dependence of the attenuation coefficient around the cut-off wavelength is in good agreement with the previous results obtained at 20 K by Fray et al. (1965) [23]. We intend to improve the cooling efficiency and fix the problem of vibrations due to the cryocooler in order to more accurately measure a variety of infrared materials at approximately 20 K; we intend to complete these measurements by the end of 2016.

ACKNOWLEDGMENTS

We are grateful to the staff of the Koyama Astronomical Observatory of Kyoto-Sangyo University for supporting us during this program. This study is financially supported by JSPS KAKENHI (16684001) Grant-in-Aid for Young Scientists (A), JSPS KAKENHI (20340042) Grant-in-Aid for Scientific Research (B), JSPS KAKENHI (21840052) Grant- in-Aid for Young Scientists (Start-up), and MEXT Supported Program for the Strategic Research Foundation at Private Universities, 2008–2012 (No. S0801061) and 2014–2018 (No. S1411028).

REFERENCES

[1] Ikeda, Y., Kobayashi, N., Kondo, S., Yasui, C., Motohara, K., and Minami, A., “WINERED: a warm near-infrared high-resolution spectrograph,” *Proc. SPIE* **6269**, 62693T (Jul. 2006).

[2] Ikeda, Y., Kobayashi, N., Kuzmenko, P. J., Little, S. L., Yasui, C., Kondo, S., Minami, A., and Motohara, K., “Diamond-machined ZnSe immersion grating for NIR high-resolution spectroscopy,” *Proc. SPIE* **7018**, 70184R (Jun. 2008).

[3] Ikeda, Y., Kobayashi, N., Terada, H., Shibayama, A., Ozawa, A., Yasui, C., Kondo, S., Pyo, T., and Kawakita, H., “High-efficiency silicon immersion grating by electron-beam lithography,” *Proc. SPIE* **7014**, 701469 (Jun. 2008).

[4] Ikeda, Y., Kobayashi, N., Kuzmenko, P. J., Little, S. L., Yasui, C., Kondo, S., Mito, H., Nakanishi, K., and Sarugaku, Y., “Fabrication and current optical performance of a large diamond-machined ZnSe immersion grating,” *Proc. SPIE* **7739**, 77394G (Jul. 2010).

[5] Ikeda, Y., Kobayashi, N., Kuzmenko, P. J., Little, S. L., Mirkarimi, P. B., Alameda, J. B., Kaji, S., Sarugaku, Y., Yasui, C., Kondo, S., Fukue, K., and Kawakita, H., “ZnSe immersion grating in the short NIR region,” *Proc. SPIE* **9151**, 915144 (Jul. 2014).

[6] Ikeda, Y., Kobayashi, N., Sarugaku, Y., Sukegawa, T., Sugiyama, S., Kaji, S., Nakanishi, K., Kondo, S., Yasui, C., Kataza, H., Nakagawa, T., and Kawakita, H., “Machined immersion grating with theoretically predicted diffraction efficiency,” *Applied optics*, **54**, 5193-5202 (Jun. 2015).

[7] Ikeda, Y., Kobayashi, N., Kondo, S., Yasui, C., Kuzmenko, P. J., Tokoro, H., and Terada, H., “Zinc sulfide and zinc selenide immersion gratings for astronomical high-resolution spectroscopy: evaluation of internal attenuation of bulk materials in the short near-infrared region,” *Optical Engineering*, **48**, 084001 (Aug. 2009).

[8] Sarugaku, Y., Ikeda, Y., Kobayashi, N., Sukegawa, T., Sugiyama, S., Enya, K., Kataza, H., Matsuhara, H., Nakagawa, T., Kawakita, H., Kondo, S., Hirahara, Y., and Yasui, C., “Development of CdZnTe immersion grating for spaceborne application,” *Proc. SPIE* **8442**, 844257 (Jul. 2012).

[9] Sarugaku, Y., Kaji, S., Ikeda, Y., Kobayashi, N., Sukegawa, T., Nakagawa, T., Kataza, H., Kondo, S., Yasui, C., Nakanishi, K., and Kawakita, H., “Infrared attenuation spectrum of bulk high-resistivity CdZnTe single crystal

in transparent wavelength region between electronic and lattice absorptions," *Journal of Electronic Materials* (2016 in prep.).

[10] Kaji, S., Sarugaku, Y., Ikeda, Y., Kobayashi, N., Nakanishi, K., Kondo, S., Yasui, C., and Kawakita, H., "The precise measurement of the attenuation coefficients of various IR optical materials applicable to immersion grating," *Proc. SPIE* **9147**, 914738 (Jul. 2014).

[11] Kuzmenko, P. J., Ikeda, Y., Kobayashi, N., Mirkarimi, P. B., and Alameda, J. B., "Reflective coating for near-infrared immersion gratings," *Proc. SPIE* **8450**, 84503O (Sep. 2012).

[12] Ikeda, Y., Kobayashi, N., Kondo, S., Otsubo, S., Hamano, S., Sameshima, H., Yoshikawa, T., Fukue, K., Nakanishi, K., Kawanishi, T., Nakaoka, T., Kinoshita, M., Kitano, A., Asano, A., Takenaka, K., Watase, A., Mito, H., Yasui, C., Minami, A., Izumi, N., Yamamoto, R., Mizumoto, M., Arasaki, T., Arai, A., Matsunaga, N., and Kawakita, H., "High sensitivity, wide coverage, and high resolution NIR non-cryogenic spectrograph, WINERED," *Proc. SPIE* (2016 in prep.).

[13] Yasui, C., Ikeda, Y., Kondo, S., Motohara, K., and Kobayashi, N., "WINERED: optical design of warm infrared echelle spectrograph," *Proc. SPIE* **6269**, 62694P (Jul. 2006).

[14] Yasui, C., Kondo, S., Ikeda, Y., Minami, A., Motohara, K., and Kobayashi, N., "Warm infrared echelle spectrograph (WINERED): testing of optical components and performance evaluation of the optical system," *Proc. SPIE* **7014**, 701433 (Jul. 2008).

[15] Terada, H., Ikeda, Y., Kobayashi, N., Yasui, C., Pyo, Tae-Soo., Usuda, T., Hayashi, M., and Kawakita, H., "High resolution spectrograph unit (HRU) for the SUBARU/IRCS," *Proc. SPIE* **7014**, 701434 (Jul. 2008)

[16] Kobayashi, N., Ikeda, Y., Kawakita, H., Enya, K., Nakagawa, T., Kataza, H., Matsuhara, H., Hirahara, Y., and Tokoro, H., "Mid-infrared high-resolution spectrograph for SPICA," *Proc. SPIE* **7010**, 701032 (Aug. 2008).

[17] Kataza, H., Sakon, I., Wada, T., Sarugaku, Y., Fujishiro, N., Ikeda, Y., Mitani, S., Ohyama, Y., and Kobayashi, N., "Performance estimation of the mid-infrared camera and spectrometer abroad SPICA," *Journal of Astronomical Instrumentation* **04**, 1550001 (Jun. 2015).

[18] Kondo, S., Ikeda, Y., Kobayashi, N., Yasui, C., Mito, H., Fukue, K., Nakanishi, K., kawanishi, T., Nakaoka, T., Otsubo, S., Kinoshita, M., Kitano, A., Hamano, S., Mizumoto, M., Yamamoto, R., Izumi, N., Matsunaga, N., and Kawakita, H., "A warm near-infrared high-resolution spectrograph with very high throughput (WINERED)," *eprint arXiv* 1501.03403 (Jan. 2015)

[19] Arasaki, T., Kobayashi, N., Ikeda, Y., Kondo, S., Sarugaku, Y., Kaji, S., and Kawakita, H., "VINROUGE: a very compact 2 – 5 μm high-resolution spectrograph with Germanium immersion grating," *Proc. SPIE* (2016 in prep.).

[20] Otsubo, S., Ikeda, Y., Kobayashi, N., Sukegawa, T., Kondo, S., Hamano, S., Sameshima, H., Fukue, K., Yoshikawa, T., Nakanishi, K., Watase, A., Takenaka, K., Asano, A., Yasui, C., Matsunaga, N., and Kawakita, H., "First high-efficiency and high-resolution (R = 80,000) NIR spectroscopy with high-blazed echelle grating: WINERED HIRES-modes," *Proc. SPIE* (2016 in prep.).

[21] Hawkins, G. J., "Spectral characterization of infrared optical materials and filters," (1998).

[22] Palik, E. D., [*Handbook of Optical Constants of Solids*], Academic Press, England (1997).

[23] Fray, S. J., Johnson, F. A., Quarrington, J. E., Williams, N., "lattice bands in germanium," *Proceedings of the Physical Society* **85**, 153 (Jan. 1965).